ORESTA

# ENHANCED POLSAR IMAGE CLASSIFICATION USING DEEP CONVOLUTIONAL AND TEMPORAL CONVOLUTIONAL NETWORKS

## Batool Anwar[1]*, Mohamed M. Morsey[2], Islam Hegazy[3], Zaki T. Fayed[4], Taha El-Arif[5]

[1,2,3,4,5]Department of Computer Science, Faculty of Computer and Information Science, Ain Shams, Cairo, Egypt.

*Research Paper*

*Abstract: A new framework in the form of Polarimetric Synthetic Aperture Radar (PolSAR) image classification, where deep Convolutional Neural Networks (CNNs) were integrated with the traditional Machine Learning (ML) techniques under a Temporal Convolutional Network (TCN) architecture, was introduced in the paper. The main aim behind this new approach is to overcome the severe limitations inherent in both deep CNN and conventional ML approaches. The application of the sliding-window strategy eliminates the necessity of requiring extensive feature extraction procedures while reducing computational complexity simultaneously. Experiments on four benchmark PolSAR datasets for C-Band, L-Band, AIRSAR, and RADARSAT-2 data attest to the framework's remarkable classification accuracies in the range of 94.55% to 99.39%. This integrated framework is thus a significant advancement in PolSAR image analysis in offering an efficient methodology that combines the strengths of deep CNNs and traditional ML, by mitigating their respective limitations. It also combines the sliding-window technique with the architecture of TCN and then yields excellent classification accuracy with no much additional computational overhead. The results obtained thus indicate a good chance of revolutionizing the state of the art in PolSAR image classification, providing crucial efficiency improvements and making applications in environmental applications stronger, across almost all kinds of fields.*

*Keywords: Deep Learning, Temporary Convolution Neural Network, Polarimetric Synthetic Aperture Radar, Support Vector Machine, Satellite Image.*

## 1. Introduction

Recently, Polarimetric Synthetic Aperture Radar, or PolSAR, has emerged as one of the most valuable tools for remote sensing because it can acquire detailed surface features for wide ranges of environmental conditions (Karachristos et al., 2024). Since

---

*Corresponding Author: Batool.anwar@cis.asu.edu.eg (B. Anwar)

multiple polarizations provide the data, PolSAR yields very complex data that would be useful for a variety of applications such as environmental monitoring, land use classification, and disaster management (Shokr & Dabboor, 2023). However, output data being this complex requires sophisticated techniques for effective analysis and classification. More recently, advancement in machine learning, especially deep learning, has promised improvements to PolSAR image classification (Han et al., 2023). However, such methods have been proven to oftentimes come hand in hand with extra bottlenecks such as high computational demands and the insistence on vast training data. Hybrid models that combine the strength of different approaches for better classification accuracy, besides reducing the overall computational burden, are gaining interest lately (Qiao et al., 2024).

Synthetic aperture radar (SAR) is a key component of modern remote sensing. It offers unparalleled information for surface features, depending on the prevailing weather conditions. Po1SAR techniques meant to enhance SAR capabilities and feature multiple orthogonal polarizations used also induces extracting data of intricate and fine resolution. Discerning and classifying Po1SAR are profoundly significant in both socioeconomic and ecological domains. A postulation of a series of methodologies was granted, (Hua, Wang, et al., 2024; Meng et al., 2024) relying often on features collected in a difficult way, which eventually restrains their efficiency. For such intrinsic limitations within conventional paradigms to be overcome, CNNs emerged during the recent epoch in the domain of visual recognition tasks. Potent due to an unrelenting appetite for unlocking the full potential of various datasets, CNNs reflect a robust architecture. This preference extends to the SAR data classification domain, supported by deep learning ( Zou et al., 2010), with a requirement for a considerable training data fraction, arousing pragmatic constraints.

This paper responds to the aforementioned exigencies by proposing a novel adaptive and compact CNN approach for accurate classification of PolSAR data. It operates directly on second-order Po1SAR data descriptors and thereby avoids necessary discrete feature preprocessing and extraction that is typically required in other approaches. This methodology extended from previous application to single- and dual-polarized SAR image classification, thus leveraging the adaptive and compact CNN framework onto the domain of PolSAR. The consequence is augmented capacity to harness an expanded repertoire of features stemming from diverse Target Decomposition theorems, courtesy of an augmented number of polarizations. The evaluation demonstrates that the adaptive and compact CNNs proposed are efficiently efficient, with the classification performance of PolSAR increased while consuming a different training data fraction-Less than 0.1% of the whole SAR corpus - and also demonstrating computational complexity that suits the real-time processing requirement. In addition to that, the designed CNN facile configuration encourages the adoption of low-resolution patches (such as From $7 \times 7$ to $19 \times 19$ pixel sliding windows, for example), which thereby reduces former challenges (Li et al., 2019).

The following sequence is a description of the organization of the paper. In section 2, the work is expounded, and in section 3, the whole methodology proposed is given in terms of data acquisition, feature extraction, and classification. In section 4, experimental results are discussed, whereas the discussion is presented in section 5. Finally, a summary of the whole work and the conclusion are given in section 6.

## 2. Related Work

Classification of PolSAR images is now an area that has attracted immense attention because such images hold much importance for environmental monitoring, land cover mapping, and disaster management. The availability of high-resolution PolSAR images also creates an imperative for the development of accurate and efficient classification techniques. Considering the inherent difficulties in PolSAR image classification, such as data complexity and demands on real-time processing, a number of approaches have been developed over the years to address them. Traditional methods usually remain based on manual feature extraction, with inherent issues associated with time-consuming and less accurate results. Promising solutions, therefore, arise in modern machine learning, especially deep learning, which automatically extract features to improve classification accuracy.

New methodologies for PolSAR image classification are both old and modern, comprising known traditional tools as well as emerging ones designed for this fast-growing area (Ferreira et al., 2024). In the initial stages, the approaches relied mainly on manual feature extraction and conventional machine learning algorithms; therefore, they were not very accurate and were very inefficient from the perspective of being computationally expensive. It is however with the increase of the complexity of PolSAR data as time passes by that the need for more advanced and automated techniques is established. Studies, such as (Imani, 2024; C. Yang et al., 2024; Zhang et al., 2024) show the utilization of diverse traditional techniques in SAR data categorization.

Stemming from various Target Decomposition (TD) approaches, a gamut of Po1SAR features is leveraged by these methods. Randon Forest (RF) and Support Vector Machines (SVMs) are among the most promising conventional classifiers, relying customarily on two SAR feature categories. Features belonging to the first category are those that can be directly extracted from SAR data, which include second-order descriptions and scattering matrices. The second category consists of methods based on features driven from target decomposition theorems. A paradigmatic shift is made noticeable within the Po1SAR classification subdomain to leverage techniques that are associated with the Deep Learning approach, and more specifically, deep CNNs have been widely adopted. Research shifts deeply into the integration of deep learning models into traditional methods for higher classification accuracy and greater computational efficiency. In fact, the evolution of methodology is consequent upon the process of challenging innovation with practicality: Classification of PolSAR images evolves keeping pace with improvements in technology and its applications, whose objectives and demands continue to change (Imani, 2024).

For Po1SAR image classification, an innovative approach that integrates online active learning with extreme learning machine (ELM) techniques was proposed by (Li et al., 2019). The methodology was designed towards improving accuracy and efficiency in the solution through the dynamics learnt from the sequential data by incorporating a discrepancy sampling strategy for informative samples. This algorithm is computationally much faster and reaches an accuracy of up to 93.47%, showcasing the algorithm's superiority over traditional methods. An innovative classification method was presented by Cao et al. (2021) for PolSAR images. In this approach, the CK-ENC is a composite kernel-based elastic net classifier that combines

the method of super pixel segmentation with composite kernel approach adapted for enhancing classification performance in cases of very small training samples. As evidenced by the results of experiments, improvements are seen substantially in terms of classification accuracy compared over a wide range of datasets. It therefore exemplifies the strength of the approach above other sophisticated techniques. From the results obtained, it can be seen that there indeed is a notable improvement that can reach as high as 97.5% in some datasets in terms of overall accuracy (OA) (Pollachom et al., 2022).

The development of efficient neural network architectures in SAR data processing is the core theme of recent developments in modern classification techniques. Recent approaches would tend to lower complexity while achieving higher accuracy, thus addressing some of the challenges brought about by the complexity nature of the SAR data (Hua, Hou, et al., 2024). Ahishali et al. (2021) applied a method that focuses on compact and efficient neural network designs for handling SAR data, emphasizing the reduction of computational complexity while maintaining high classification accuracy. The methodology involves adapting CNN architectures for SAR image processing, including techniques for handling SAR data exceptional features, like speckle noise as well as varying polarizations (Yadav et al., 2022).

The focus on creating a comprehensive Po1SAR image analysis dataset was clear in (Wang et al., 2022). The new dataset was aimed to overcome the shortcoming of current datasets such as higher complexity and larger scale for complex terrain, which will promote the development of advanced algorithms for terrain segmentation. For these purposes, their work proposes the collection and annotation of Po1SAR images, utilizing satellite GaoFen-3 as the imaging data provider and a large-scale manual annotation procedure to guarantee correct labels on the terrain category. With 2000 high-resolution image patches categorized into six terrain types, the AIR-PolSAR-Seg dataset is very valuable for PolSAR terrain segmentation research. Multicategory terrain segmentation experiments demonstrate that deep learning methods considerably outperform traditional approaches; the mean Intersection over Union (mIoU) is between 44.23% and 52.58%, and OA is between 75.53% and 77.46%. Deep learning methods perform even more superiorly such as OA ranges from 98.48% to 98.83% and mIoU scores from 85.80% to 89.29%. In building segmentation, deep learning methods attained OA scores ranging from 82.43% to 83.84% and mIoU scores ranging from 85.80% to 89.29%, thus indicating that these methods are remarkably superior to deal with category imbalances as well as complicated scenes in the AIR-PolSAR-Seg dataset.

A novel approach was proposed in Chen et al. (2023) for enhancing neural network classification of PolSAR image. This Wishart Locally Constrained Expansion (WLCE) method increases the efficiency of the training dataset through Wishart distribution and makes use of spatial correlations to expand samples. Semi-supervised PolSAR image classification overcomes the challenge of the lack of sufficient labelled data so that overall accuracy can be significantly improved across benchmark datasets. The accuracy reaches up to 97.43%, as demonstrated through extensive experiments and comparisons with the existing techniques (Li, 2022).

*Table 1: Presented Studies for PolSAR Images Classification*

| Authors and Year | Dataset | Methodology | Classification Method | Result (Performance) |
|---|---|---|---|---|
| (Li et al., 2020) | AIRSAR L-Band (San Francisco Bay, Flevoland), RADARSAT-2 C-Band (San Francisco Bay, Flevoland) | Online Active Extreme Learning Machine with Discrepancy Sampling | Extreme Learning Machine (ELM) | Improved Efficiency and Accuracy A = 93.47% |
| (Cao et al., 2021) | Various PolSAR Datasets | Super Pixel-Based Composite Kernel and Elastic Net | Composite Kernel-Based Elastic Net Classifier | Demonstrates Significant Accuracy Improvement A = 97.5% |
| (Ahishali et al., 2021) | AIRSAR L-Band (San Francisco Bay, Flevoland), RADARSAT-2 C-Band (San Francisco Bay, Flevoland) | Compact and Adaptive CNN | Convolutional Neural Network | A = 85.33% on AIRSAR L-Band And A = 81.33% on RADARSAT-2 C-Band |
| (Ahishali, & Kiranyaz et al., 2021) | Various SAR Datasets | Adaptive CNNs for SAR Image Classification | Convolutional Neural Network | Overall Accuracy Ranging 92.33% to 99.39% |
| (Wang et al., 2022) | GaoFen-3 satellite imagery (Hangzhou, Zhejiang province, China) | AIR-PolSAR-Seg: A Large-Scale Data Set for Complex-Scene PolSAR Images | SVM | Overall, Accuracy is between 98.48% and 98.83%. |
| (Chen et al., 2023) | AIRSAR L-Band (San Francisco Bay, Flevoland), RADARSAT-2 C-Band (San Francisco Bay, Flevoland | Wishart Locally Constrained Expansion (WLCE) | Neural Network with WLCE | A = 97.43% |
| (Fang et al., 2023) | Flevoland-15, Flevoland-14, Oberpfaffenhofen, San Francisco | HA-EDNet with Self-Attention and Selective Kernel Module | Hybrid Attention-Based Encoder–Decoder Network | 99.39% Overall Accuracy (Flevoland-15 Dataset) |

Employing a hybrid attention-based encoder-decoder network (HA-EDNet) by a state-of-the-art approach was proposed in (Fang et al., 2023) for PolSAR image classification. Self-attention mechanisms are incorporated into this method for enhancing the model's capacity of focusing on suitable features within images, for a more meticulous classification. These experiments have been conducted in multiple datasets in which high performance has been discovered with respect to earlier

methods. The proposed algorithm carried out the tests from various datasets and revealed improvement in average accuracy (AA), Kappa coefficient, and overall accuracy (OA) when compared to the traditional methods. In a few data sets, a 5% growth was reported in the counterpart OA, thereby proving that the extended training sample method was efficient in enhancing the classifier's generalization and robust capabilities. As more evidence is in the results, satisfactory performance can be encountered using the relatively small amount of original training samples. It therefore can be considered as an excellent method for Po1SAR image classification, assuming the scarcity within the annotated data (Shabayek et al., 2022).

In recent years, there is indeed a clear trend in pursuing deep learning classification over PolSAR imagery, especially with the use of CNNs. Researchers today are more focusing on innovative techniques that don't only improve upon accuracy but also address certain limitations in computational and dataset sizes. The studies presented in Table 1 manifest that a significant shift can be witnessed in the Po1SAR image classification field towards deep learning methodologies, especially in the leverage of deep CNNs. The researchers have started exploring new avenues, such as compact adaptive CNN architectures, composite kernel-based classifiers, and online active learning with extreme learning machines. These approaches aim at better classification accuracy over the problem of the limited size of a dataset and improve computational efficiency. To increase attention mechanisms and hybrid approaches, including CNN training with Wishart classification, reveals the necessity of refining methodologies in achieving accuracy and efficiency while developing innovation in PolSAR image classification research (Al Doghan & Piaralal, 2024).

## 3. Methodology

The methodology as a whole is possibly divided into four primary phases, which encompass data collection, initial preparation, feature extraction, and categorization or classification.

### 3.1 Data Acquisition

The first phase, data collection, involves using four established PolSAR datasets collected online. Two of these datasets were obtained from an aerial system, specifically the NASA/Jet Propulsion Laboratory AIRSAR (Moon et al., 2010). In Moon et al. (2010), the Canadian Space Agency RADARSAT-2, a spaceborne system, was used for acquiring the two datasets remaining. These diverse datasets make the study have a good basis for in-depth analysis and incorporation of both aerial and spaceborne systems. The use of both AIRSAR and RADARSAT-2 datasets contributes to a well-balanced approach by integrating data from alternative acquisition methods. The choice supports an in-depth analysis of PolSAR image classification founded on long-standing sources from platforms of both aerial and spaceborne nature.

*Table 2: Dataset used in the Proposed Study*

| Name | System & Band | Abbr. | Date Incident |
|---|---|---|---|
| SF Bay | AIRSAR_L | SFBay_L | 10-60 Degrees |
| SF Bay | RADARSAT-2C | SFBay_C | 30 Degrees |
| Flevoland | AIRSAR_L | Flevo_L | 40 – 50 Degrees |
| Flevoland | RADARSAT-2C | Flevo_C | 30 Degrees |

*Table 3: Classes Number, the Final Entire Ground Truth (GTD) Size, and Training Size*

| Name | Dimensions | Classes | Train Size Per class | Total GTD Size |
|------|-----------|---------|---------------------|----------------|
| SF Bay | 900 x 1024 | 5 | ~292 | 123459 |
| SF Bay | 1426 x 1876 | 5 | 500 | 252500 |
| Flevoland | 750 x 1024 | 15 | 120-480 | 209979 |
| Flevoland | 1639 x 2393 | 4 | 500 | 202000 |

In California, USA, San Francisco Bay, the first research region is situated, observations there are made by using C-band (SFBay_C) and L-band (SFBay_L) frequencies as shown in figure. 1, and 2 respectively. The second area of interest is the Flevoland region in the Netherlands, with data collection made by using C-band (Flevo_C) and L-band (Flevo_L) frequencies as shown in Figures 3 and 4. The pixels set, present in every image, is divided into testing and training sets representing regions and types of areas classified. In addition, every image typically consists of several channels that correspond to different polarizations and their combinations. Every channel within a PolSAR image provides unique information related to the structure and composition of the scene captured. All the channels used in most of the studies used for this study are capable of defining various features in the image. The lowest number of channels that is used in this study is three, while the highest number of channels that is used in this study is six, and this is because the standard applied in most of the work depicts in the related studies.
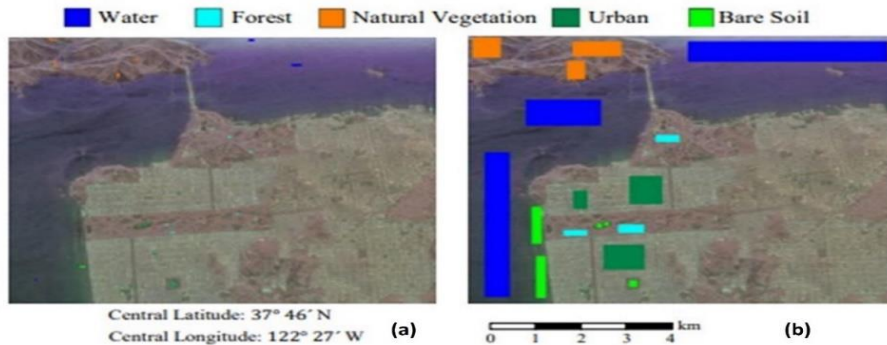


*Figure 1: (a) Training Pixel Samples (b) Non-Overlapping Test Regions After Preprocessing the SFBay L PolSAR Image.*
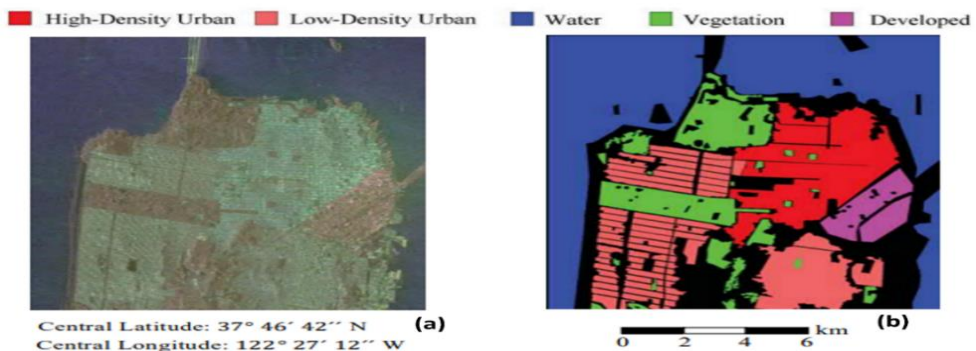


*Figure 2: SFBay_C PolSAR Image: (a) PauliRGB Representation, (b) Associated Ground Truth Dataset with Class Labels on the Right After Preprocessing.*
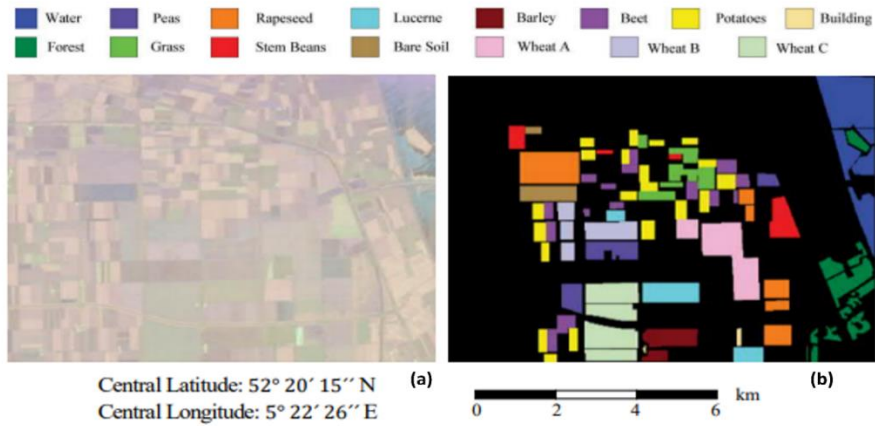
Figure 3: Shows the Flevo_L PolSAR Image: (a) After Scaling and Logarithmic Transformation(b) With Distinctive RGB Colors in Every Class, Ground Truth Land Cover Dataset Can Be Seen.
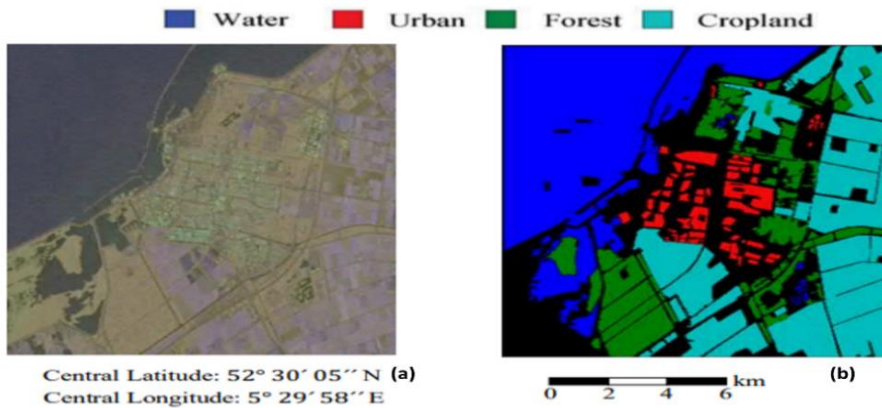


Figure 4: The Flevo_C PolSAR Image: (A) After Logarithmic Transformation and Scaling, (B) Ground Truth Land Cover Dataset With Unique RGB Colors For Each Class.

### 3.2 Pre-Processing

The pixel gathered from the images are converted to float and decimal values before any feature extraction. Also, it important to mention that pixels are normalized between 0 to 1 and any missing or noisy data are removed from the entire four benchmark datasets.

### 3.3 Feature Extraction using TCN

Recently, TCN excelled in many applications in various domains, including traffic forecasting, sound event detection, probabilistic prediction, etc. Initially introduced (Lara-Benítez et al., 2020; Lea et al., 2016), TCN demonstrated exceptional performance in tasks such as video action prediction, classification, and segmentation. Through two main steps, TCN operation can be seen. In the first step, low-level features are computed by employing CNN models, which encode spatial-temporal

203

information. In the second step, passing of these low-level features is made into a model, which can be RNN or CNN for high-level temporal patterns to be captured. In this case, the preprocessed pixels are fed into TCN as sequential features, which in turn are transformed into a probability distribution. Inputs pass through four stacks of residual blocks with two weight normalization layers, two dilated causal convolution layers, one ReLU activation layer, and an optional convolutional layer, followed by two dropout layers. The very first residual block is different because it uses three dilated causal convolution layers (Guo & Yuan, 2020).

Dilated Causal Convolutional Layer: An input sequence with particular length can be taken by this layer in the TCN model for generating a same-length output. It is given a "causal" name since activations from future time steps cannot be depended on by activations produced at a specific time step. Input to TCN is defined by $Y=[y\_1,y\_2,\ldots\ldots,y\_i]$ and a filter $f:\{0,\ldots,k-1\}$. The following equation is used for defining the dilated casual convolutional operation on the ith point of Y is defined using the following equation:

$$C(y\_i)=\sum\_{(a=0)}^{(k-1)} 〚f(a)〛 \text{ -}y\_{(i-a.d)} \qquad (1)$$

Where the dilation factor is d, filter size is k, and past direction is indicated by i-a.d. In other words, Y is kept as the input sequence by the first layer, whereas the former layer output in higher layers is indicated by Y. A dilation factor is there for every dilation convolutional layer, and this factor increases exponentially by a factor of 2. The dilation factor is used so as to perform the convolution with the order pixel in a specific order based on the dilation value. For example, if the value of the dilation factor 2 then there will be a convolution of the filter value with the five pixel and the tenth pixel etc.

Weight Normalization Layer (WN): To every dilated convolutional layer, an application of this layer is conducted. For this purpose, a particular learning scaling parameter is used for weights normalization. In the equation (2), a definition is given of the weight normalization operation equation:

$$o\_j=s\_j (W\_j * x)/(|(|W\_j|)|\_F+ \epsilon)+j \qquad (2)$$

The WN layer input is x, the WN layer output is o, the scale is defined as $s\_j$, the bias is set as j, the constant employed for numerical stability is $\epsilon$, the layer's weight and the weights Frobenius norm are $W\_j$ and $|(|W\_j|)|\_F$, respectively, for the output channel j, while the convolution operator is *.

The residual block to which the input is submitted undergoes a totally optional 1x1 convolution layer whose subsequent combination will be made with the output of the residual block. Its application is made at the instance where no matching between the number of channels in the input and the number of channels in the output is found. For all other residual blocks, the same process is repeated again. At last, after the four blocks have been processed, the output of the fourth block is passed through one ReLU activation layer, a classification layer, one Softmax layer and two fully connected layers. Main parameters overview of TCN can be found in Figure 5. This figure comprises: dilation factors, number of input channels, and the number of blocks.
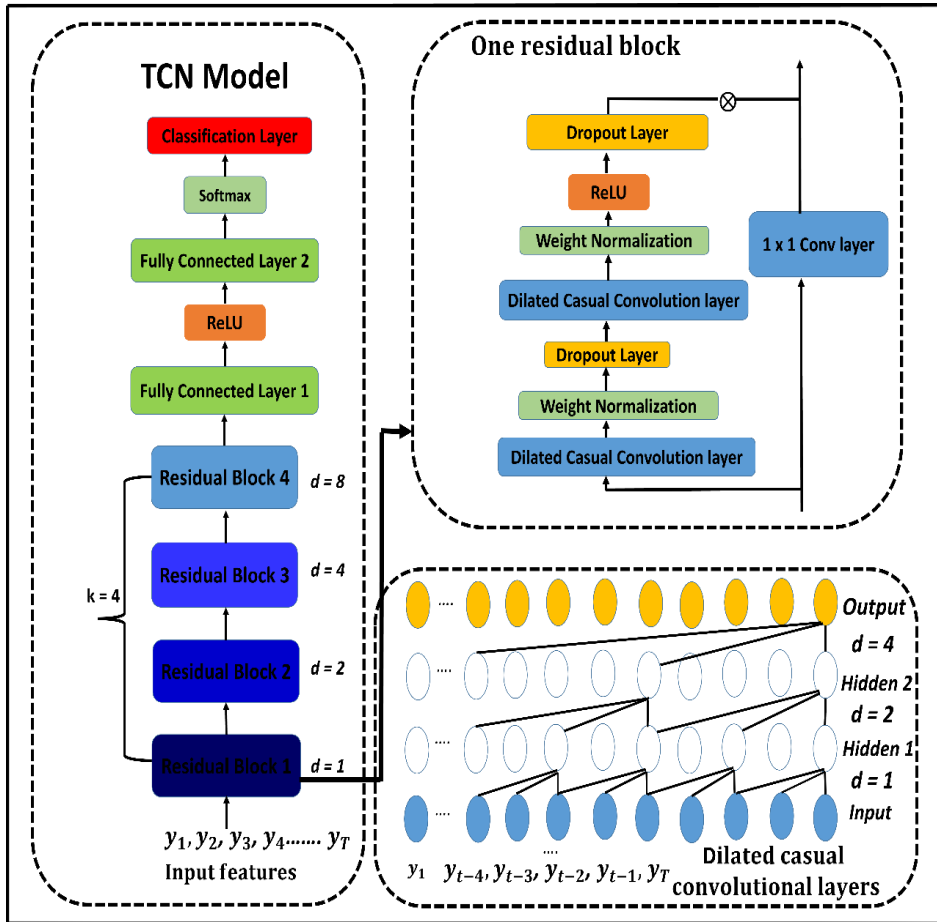
*Figure 5: Entire TCN Architecture*

### 3.4 Classification using Support vector machine (SVM)

SVM is one of the most used techniques of machine learning; it offers very useful solutions to many problems. Übeyli (2007) proposed SVM which is employed in regression, classification, and several other applications. SVM key functionality is its mapping of input features into a high dimensional feature field by a nonlinear employment. A quadratic optimization problem is SVM training process. The following equation is used for defining the hyperplane construction:

W^T x+b =0                    (3)

Where x is the input feature vectors, b is the bias factor, the hyperplane coefficients vector is W. The aim is margin maximization between the nearest point and hyperplane. Then, the SVM begins to learn the main parameters which are W and b by solving a specific optimization problem defined using the following equation:

min 1/p W^T W+C∑_(i=1)^P▒E_i      s.t{■( 〚(W.x+b)≥〛 _ 1-E_i@E_i≥0,i=1…..p)┤

(4)

Where W^T W is the manhattan norm, the penalty parameter is defined by C, and E_ is the cost function. This optimization problem is solved using sequential minimal optimization (SMO), and this requires choosing the kernel function correctly. In this study, the polynomial kernel function is the applied kernel function. The kernel function applied is the polynomial kernel function. The approach that combines the binary SVM classifier is known as error-correcting output codes (ECOC). In this approach, the SVM is trained till $2^{(n-1)}-1$ (where the classes number is n), with each targeting variant classes combination separation. Each of them is aimed at the separation of a variant combination of classes. The final multi-class SVM output is the combination of all these separable SVM classifiers results.

## 4. Experimental Setup

The theme of the paper addresses the analysis and classification of PolSAR images using advanced techniques of feature extraction. Using multiple datasets, this work is aimed at enhancing classification accuracy while probing into the effectiveness of several levels of features. This paper discusses four datasets, where each dataset is comprised of three feature levels: 6, 4, and 3. For each dataset, it has specific numbers of training and testing features as shown in Table 4. The extracted features from TCN model are then used to train SVM for classification. Training and testing pixels originated from one source image but were taken across different channels. There are two primary reasons for training on pixels {Liu, 2022 #28}. First, it used only one image per dataset, and also, every pixel belongs to a definite region meant for classification. All experiments were conducted on a laptop with an Intel Core i7-8565 processor, 12 GB of RAM, and an NVIDIA GeForce GTX 310M graphics card, with 2 GB of dedicated memory, running under MATLAB and Weka software. In experiments, each picture is composed of multiple channels that provide information about a certain picture for several polarizations. The size of each channel for all channels corresponds to the sizes of the image.

*Table 4: Number of Training and Testing Features*

| Dataset | No of Training Pixels | No of Testing Pixels |
|---------|----------------------|---------------------|
| sfbay_l | 1462 | 121997 |
| sfbay_c | 2500 | 250000 |
| flevo_l | 4211 | 204023 |
| flevo_c | 2000 | 200000 |

### 4.1 Experimental Results

In this section, the work present the results obtained from our experiments. This section discuss how the TCN together with the SVM classifier shows high effectiveness. The set of performance metrics across different datasets reveals the impact of different feature levels on achieving classification accuracy. From these results, it could be inferred that which is more useful for the model or how well can it perform. The provided results showcase the performance of a TCN combined with an SVM classifier on various datasets with different numbers of features. Let's break down and comment on these results measured in table 5.

*Table 5:  Results Obtained from the Combination of the TCN and SVM*

| Datasets | No. of Features | TCN + SVM Classifer | | | | | | | | | | | |
|---|---|---|---|---|---|---|---|---|---|---|---|---|---|
| | | A | TP | FP | K | TPR | FPR | P | R | F1 | MCC | ROC | RPC |
| sfbay_l | 6 | 95.17 | 116111 | 5886 | 0.9 | 0.952 | 0.012 | 0.950 | 0.952 | 0.951 | 0.943 | 0.996 | 0.968 |
| | 4 | 95.31 | 116279 | 5718 | 0.9 | 0.953 | 0.017 | 0.952 | 0.953 | 0.952 | 0.941 | 0.996 | 0.974 |
| | 3 | 94.55 | 115356 | 6641 | 0.8 | 0.946 | 0.018 | 0.945 | 0.945 | 0.945 | 0.929 | 0.982 | 0.920 |
| sfbay_c | 6 | 99.71 | 249290 | 710 | 0.9 | 0.997 | 0.001 | 0.997 | 0.997 | 0.997 | 0.996 | 1.000 | 1.000 |
| | 4 | 99.55 | 248843 | 1105 | 0.9 | 0.996 | 0.001 | 0.996 | 0.996 | 0.996 | 0.999 | 0.998 | 0.993 |
| | 3 | 99.47 | 248677 | 1323 | 0.9 | 0.995 | 0.001 | 0.995 | 0.995 | 0.995 | 0.993 | 1.000 | 1.000 |
| flevo_l | 6 | 86.45 | 176394 | 27629 | 0.85 | 0.865 | 0.011 | 0.874 | 0.865 | 0.866 | 0.856 | 0.986 | 0.919 |
| | 4 | 84.72 | 172867 | 31156 | 0.83 | 0.847 | 0.012 | 0.858 | 0.847 | 0.849 | 0.838 | 0.976 | 0.790 |
| | 3 | 85.76 | 174977 | 29046 | 0.84 | 0.858 | 0.011 | 0.864 | 0.858 | 0.859 | 0.848 | 0.985 | 0.912 |
| Flevo c | 6 | 99.92 | 199846 | 154 | 0.9 | 0.999 | 0.000 | 0.999 | 0.999 | 0.999 | 0.999 | 1.000 | 1.000 |
| | 4 | 99.85 | 199715 | 285 | 0.9 | 0.999 | 0.000 | 0.999 | 0.999 | 0.999 | 0.998 | 0.999 | 0.998 |
| | 3 | 99.87 | 199748 | 252 | 0.9 | 0.999 | 0.000 | 0.999 | 0.999 | 0.999 | 0.998 | 1.000 | 1.000 |

In terms of sfbay_l dataset, with 6 features the TCN + SVM classifier for the sfbay_l dataset with six features achieved a true positive (TP) count of 116,111 and a false positive (FP) count of 5,886. The Kappa statistic (K) McHugh (2012) for this configuration was 0.9. A 0.012 false positive rate (FPR) and 0.952 true positive rate (TPR) are demonstrated by the classifier. Precision (P) was calculated at 0.950, with a recall (R) of 0.952, leading to an F1 score of 0.951. The Matthews correlation coefficient (MCC) Chicco and Jurman (2020) was 0.943. The performance on the ROC and PRC metrics were 0.996 and 0.968, respectively, while with 4 features, the classifier had a slightly improved performance with a TP count of 116,279 and an FP count of 5,718. The Kappa statistic remained at 0.9, but the TPR improved marginally to 0.953, while the FPR was 0.017. Precision and recall were both at 0.952, maintaining an F1 score of 0.952. The MCC was 0.941, with ROC and PRC scores of 0.996 and 0.974, respectively, whereas, with 3 features the classifier achieved a TP count of 115,356 and an FP count of 6,641. The dropping of the Kappa statistic was to 0.8, the FPR was 0.018 and the TPR was 0.946. Recall and precision were at 0.945, and this leads to a 0.945 F1 score. At 0.929, the MCC was lower, and PRC and ROC were 0.920 and 0.982, respectively.

The classifier, in the sfbay_c dataset with six features, has achieved count 710 FP and 249,290 TP. 0.9 has been recorded as the high Kappa statistic, while FPR and TPR have been 0.001 and 0.997, respectively. Both recall and precision have recorded 0.997, with a resulting F1 score of 0.997. MMC recorded 0.996, while both ROC and PRC are perfect at 1.000. A classifier that had four features scored a count of 1,105 FP and 248,843 TP. The Kappa statistic was kept at 0.9, and FPR scored at 0.001 and TPR kept at 0.996. F1, precision, and recall scores made 0.996 each. MCC scored 0.999 with PRC scores at 0.993 and ROC scores at 0.998. For three features, the classifier made a total count of 1,323 FP and 248,677 TP. The value of kappa statistic registered was 0.9 with a 0.995 TP, and such a low FPR of 0.001; recall, F1, and precision scores all registered 0.995. With perfect 1.000 PRC and ROC scores, MCC registered 0.993.

The dataset classifier of the flevo_1 with six features achieved a count of 27,629 FP and 176,394 TP. The Kappa statistic reached 0.85 while the FPR and TPR reached 0.011 and 0.865 respectively. Recall reached 0.865 and precision reached 0.874 and it resulted in a 0.866 F1 score. With 0.919 PRC scores and 0.986 ROC scores, MCC reached 0.856. The classifier was provided with 172,867 TP counts while four features were available. The FP counts reached 31,156. The values for FPR were recorded at 0.012 and TPR at 0.847. The Kappa statistic reached 0.83. Recall recorded 0.847 while precision recorded 0.858, and this culminated into a 0.849 F1 score. Respective to their PRC scores at 0.790 and ROC scores at 0.976, the MCC recorded 0.838. The three features obtained a count of 29,046 FP and 174,977 TP by the classifier. FPR recorded at 0.011, TPR recorded at 0.858, and the Kappa statistic recorded at 0.84. The three features obtained a count of 29,046 FP and 174,977 TP by the classifier. FPR recorded at 0.011, TPR recorded at 0.858, and the Kappa statistic recorded at 0.84. Both Recall and precision made a score of 0.864 that led to 0.859 F1 score. 0.912 PRC scores. The PRC and ROC scores were 0.912 and 0.985 respectively, with MCC recorded at 0.848.

154 FP count and 199,846 TP count was recorded by the classifier in the flevo_c dataset with six features. FPR recorded 0.000 and TPR recorded 0.999, respectively, Kappa statistic recorded 0.9. Recall and precision recorded 0.999, that led to 0.999 F1 score. MCC recorded 0.999 with 1.000 perfect PRC and ROC scores. Four features the

classifier attained a count of 285 FP count and 199,715 TP count. Corresponding to 0.000 FPR and 0.999 TPR respectively, the classifier recorded a 0.9 Kappa statistic. The recall of the classifier recorded 0.999 while the precision also recorded 0.999 and this resulted in 0.999 F1 score. At respective 0.998 PRC and 0.999 ROC scores, the MCC recorded 0.998. With 1.000 perfect PRC and ROC scores, the MCC recorded 0.998. The accuracy achieved was 99% for the fourth and second datasets, while for the first dataset, the achieved accuracy is 95.2%. In the third dataset, the lowest accuracy reached was with 86.5% performance, and this is due to the reason of classifying the number of classes.

## 4.2 Confusion Matrix

With this view, the work now detail the analysis for the matrices generated from the four datasets, providing a detailed view of how well the SVM performs on the test data. The work can hence evaluate how well the combined TCN and SVM approach may do in properly classifying the data by going through these metrics. In this section, in addition to the deep learning model, the confusion matrices are presented, as extracted from the employed four datasets. These confusion matrices are mainly for providing an overview of how well the SVM performs on the test data. It gives an idea of how the overall SVM performance has been obtained. The combined confusion matrices depicted in Figures 6, 7, 8, and 9 illustrate how the proposed TCN with SVM model performed very effectively.



*Figure 6: Sfbay_l Performance using TCN Combined with SVM Classifier Based on 6, 4, and 3 Channels*

## flevo_c Dataset Channel 6

| | Target 0 | Target 1 | Target 2 | Target 3 | |
|---|---|---|---|---|---|
| **0** | 50009 / 25.0% | 2 / 0.0% | 0 / 0.0% | 0 / 0.0% | 100.0% / 0.0% |
| **1** | 0 / 0.0% | 49844 / 24.9% | 156 / 0.1% | 0 / 0.0% | 99.7% / 0.3% |
| **2** | 0 / 0.0% | 71 / 0.0% | 49912 / 25.0% | 17 / 0.0% | 99.8% / 0.2% |
| **3** | 0 / 0.0% | 0 / 0.0% | 6 / 0.0% | 49994 / 25.0% | 100.0% / 0.0% |
| | 100% / 0.0% | 99.9% / 0.1% | 99.7% / 0.3% | 100.0% / 0.0% | 99.9% / 0.1% |

Output Class (y-axis), Target Class (x-axis)

## flevo_c Dataset Channel 4

| | Target 0 | Target 1 | Target 2 | Target 3 | |
|---|---|---|---|---|---|
| **0** | 50010 / 25.0% | 1 / 0.0% | 0 / 0.0% | 0 / 0.0% | 100.0% / 0.0% |
| **1** | 0 / 0.0% | 49938 / 25.0% | 62 / 0.0% | 0 / 0.0% | 99.9% / 0.1% |
| **2** | 0 / 0.0% | 112 / 0.1% | 49789 / 24.9% | 99 / 0.0% | 99.6% / 0.4% |
| **3** | 0 / 0.0% | 6 / 0.0% | 5 / 0.0% | 49989 / 25.0% | 100.0% / 0.0% |
| | 100% / 0.0% | 99.8% / 0.2% | 99.9% / 0.1% | 99.8% / 0.2% | 99.9% / 0.1% |

Output Class (y-axis), Target Class (x-axis)

## flevo_c Dataset Channel 3

| | Target 0 | Target 1 | Target 2 | Target 3 | |
|---|---|---|---|---|---|
| **0** | 50011 / 25.0% | 0 / 0.0% | 0 / 0.0% | 0 / 0.0% | 100% / 0.0% |
| **1** | 0 / 0.0% | 49980 / 25.0% | 20 / 0.0% | 0 / 0.0% | 100.0% / 0.0% |
| **2** | 0 / 0.0% | 99 / 0.0% | 49876 / 24.9% | 25 / 0.0% | 99.8% / 0.2% |
| **3** | 0 / 0.0% | 0 / 0.0% | 10 / 0.0% | 49990 / 25.0% | 100.0% / 0.0% |
| | 100% / 0.0% | 99.8% / 0.2% | 99.9% / 0.1% | 100.0% / 0.0% | 99.9% / 0.1% |

Output Class (y-axis), Target Class (x-axis)

*Figure 7: Sfbay_c Performance using TCN Combined with SVM Classifier Based on 6, 4, and 3 Channels*

In Figure 6, the first matrix, confusion matrix is examined. It is structured with target classes along the x-axis and the predicted classes which the classifier generates along the y-axis. Color-coding is applied, using green regions to refer to correctly classified images, and red regions for those classified wrongly. The top and the first row of the matrix comprise six major cells. The first cell will carry an integer, that counts the number of times correctly classified in this instance. For the first class, there are 78653 such integers. The percentage accompanying is obtained by dividing the above count by the total number of features, which is 121997. This pattern continues in the first row of the cells, which is representation for several classes; the second last cell in the first row is the count of number of wrongly classified instances.

This trend is repeated for rows 2 through 5, in that they display performance for their respective classes. As each has two percentages, cells are added to the bottom row of the confusion matrix. Each cell first percentage is green, indicating it as precision, while its red percentage is the false discovery rate. Similarly, there also exist two percentages in the last column of the matrix. The percentage in green represents sensitivity. That is, the rate of true negatives in red. Lastly, two percentages are represented by the cell on the lower right of the confusion matrix. One in red and the other in green. The red percentage represents the overall rate of misclassified features; percentage in green, overall accuracy of the entire dataset being classified correctly.
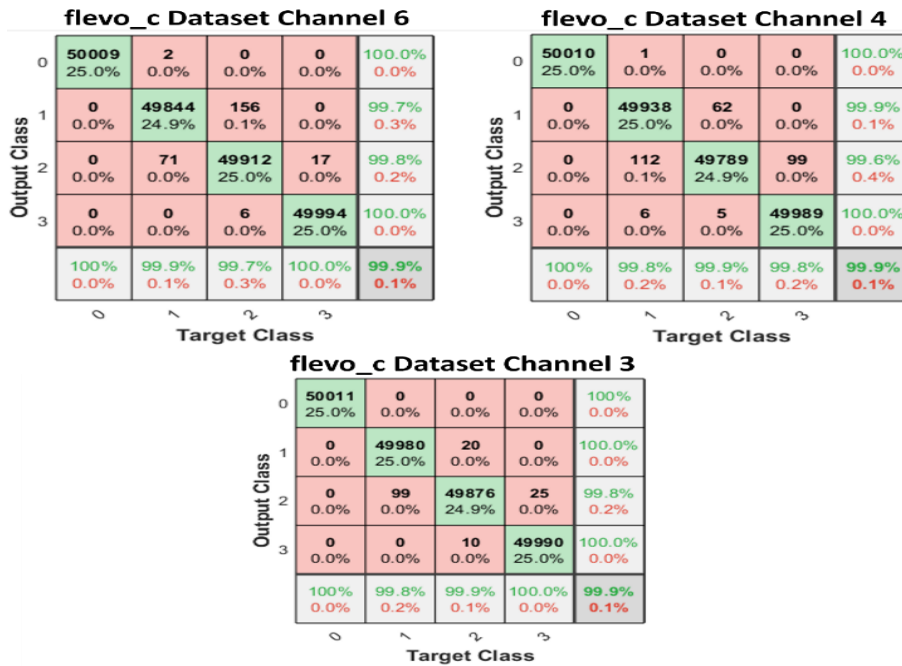
*Figure 8: Flevo_l Performance using TCN Combined with SVM Classifier Based on 6, 4, and 3 Channel*
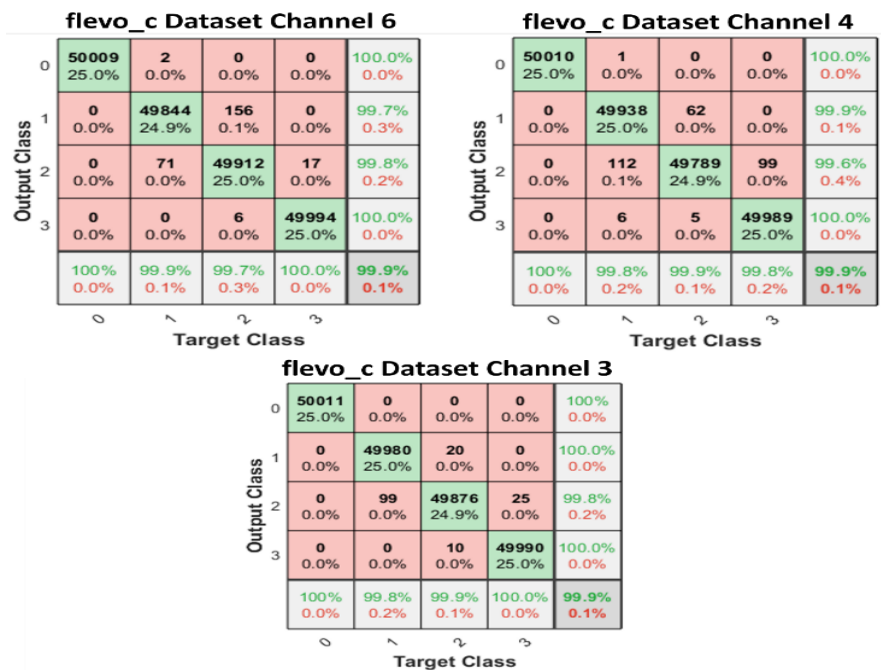


*Figure 9: Flevo_c Performance using TCN Combined with SVM Classifier Based on 6, 4, and 3 Channel*

211

## 5. Discussion

The entire field of PolSAR image classification underwent drastic changes with the addition of sophisticated machine learning techniques, especially deep models. Although classical approaches formed a foundation, a whole array of bottlenecks was encountered, including difficulty in processing large and complex datasets and being highly reliant on the extraction of manual features. With the advent of deep learning, prospects opened up for more automated, accurate classification schemes for large volumes of high-dimensional PolSAR data. However, these advancements carry the challenges of many deep learning models that require extra demand on computation and additional large datasets for training. This study pivots to pioneer the hybrid framework by joining TCNs with SVMs, which improves its classification performance and avoids the problem of computational inefficiency in real-time applications. This way, the model presents a highly efficient solution for PolSAR image classification using TCNs' ability to capture spatial-temporal features and SVM's robustness in the classification. The salient feature of the framework, sliding-window technique, also reduces computational demands and is, therefore, quite suitable for practical implementation on a large scale.

Results of this study reveal that TCNs-SVMs hybrid classification is highly efficient for PolSAR images. This kind of approach uses the complementary strength of both the models - TCNs in capturing complicated spatial and temporal patterns while the SVMs do perform strongly for classification. Experimental results over varied accuracy between 86.45% and 99.92% demonstrate the model performs exceptionally well when compared across different datasets, even with relatively few training samples. The sliding window method used in this paper reduces computational expense and makes it much more suitable for real-time applications than traditional deep learning strategies. In addition, residual blocks and dilated causal convolutions in the TCN architecture make it possible to deal with long sequences without loss of accuracy. Quantitative results also show that even with fewer input features, the proposed TCN-SVM framework can achieve satisfying accuracy, and thus is a more efficient solution for classification tasks of PolSAR images. It observes a consistent low false positive rate for the confusion matrices obtained for each dataset, which will be a good sign that the model is accurate for classifying PolSAR data. One of the strengths of the TCN-SVM framework is that it does manage to be highly classificatory with fewer features, especially as reflected in the results obtained for the SF Bay dataset. Even with reduced feature sets, the model still showed over 94% in its classification accuracy, thus further proving its efficiency. This reduction in feature dependency not only speeds up the classification process but also reduces the computational burden and, therefore, is highly applicable to real-time or near-real-time operations.

Performance on the SF Bay and Flevoland datasets clearly demonstrates flexibility in the proposed method for different geographic regions and conditions of imaging. Nevertheless, promising results in general are worth emphasizing that performance might vary with the complexity of the datasets at hand. For example, dataset Flevoland has a higher number of classes; thus, it faces much greater challenges in the classification process and, therefore slightly impacts accuracy. These experiments present the fact that although the model TCN-SVM is highly effective, there still remains room for improvement concerning working with more difficult datasets as well as handling class imbalances. Another practical dimension is that it has

minimized the requirement of intensive feature extraction to become successful as proved with the framework's remarkable success using much leaner feature sets. The efficiency justifies its perfect application in the real-time processing application field where rapid image classification is a must. Thus, this proposed model can be accredited as a practical answer to the challenge of PolSAR image classification especially in those applications involving limited or scarce computational resources.

Beyond these general findings, a closer examination of the technical aspects further highlights the robustness and scalability of the TCN-SVM framework. But, to further expand the discussion, it would be interesting to go more into the depth of technical matters concerning the TCN-SVM hybrid model, especially the adaptability and scalability towards different PolSAR datasets. In this paper, TCNs present an efficient way to handle sequential and spatial-temporal data, which is an important requirement in PolSAR image classification because of the spatial orientation of the features with different polarizations. This task particularly suits TCNs as they can model long-range dependencies without increasing the computational burden in comparison to traditional RNNs or other deep learning approaches. Dilated causal convolutions within the TCN framework assist the model in trying to catch small detailed details from PolSAR images without losing important information over time. This preserves the spatial and temporal patterns of PolSAR data, because minor but informative polarization variations may cause the interpretation of the terrain to change. Other residual connections in TCNs boost gradient flow at training; therefore, deeper networks can be efficient, a factor necessary for achieving high accuracy across several datasets, like SF Bay and Flevoland.

In addition, the SVM classifier introduced after the feature extraction step introduces a robustness feature in the classification process. The reason is that SVM can very well handle the high dimensional feature space generated by the TCN. This will have the advantage of not easily being affected by noise or outliers since it was in most cases in the problem studied here, with the existence of speckle noise and other distortions. This has led to the consistently low false positive rates across the different datasets which makes the model a feasible device for real-world applications. Another technical strength of the TCN-SVM framework is that it can work well even when using smaller training datasets. Unlike most other deep learning models which would not be able to attain good accuracy with small datasets, the proposed model is robust in the absence of large amounts of labelled data. This is especially relevant in applications involving remote sensing, where it would be very challenging and expensive to obtain labelled PolSAR data. A sign that the model has the possibility for transfer to domains or datasets where substantial feature engineering or expensive data pre-processing are not feasible is indicated when it proves to be accurate with a reduced feature set.

The sliding-window approach used in this study diminishes the computational costs and lightens up the model such that it can be applied in real-time. With the sliding window, the model computes on small patches of images to get a more accurate classification while intaking reduced data at a given time. This modular approach is beneficial when working with large-scale datasets or when deploying the model in resource-constrained environments, such as satellite-based systems or field operations for disaster management. Practically, the TCN-SVM framework has the potential to be deployed in fields such as environmental monitoring, urban planning, and defence. The adaptability of the model to other imaging conditions, as well as different geographic locations, makes it particularly useful in tasks like land use

classification and deforestation tracking, or even infrastructure development. Additionally, its efficiency under limited computational resources offers it a huge potential in disaster response operations where real-time data, such as SAR data, is quickly needed for rapid and reliable classification. Overall, the technical innovations of this study, ranging from the combined use of TCN's capacity to extract features temporally, with SVM's robust classification, dilated convolutions, and the sliding-window approach, contribute to a more scalable and efficient solution for PolSAR image classification. Further research may further delve into the model's potential with even more diverse datasets and integrate the best of advanced machine learning techniques to enhance classification accuracy and computational efficiency further.

## 6. Conclusion

It combines a novel approach of CNNs applied to TCN in the classification of PolSAR data. Compared to deep networks requiring very huge training samples and large patches, the TCN consumes low computation complexity and less human intervention, allowing it to be an excellent real-time application. Generally, it has the potential in improving both segmentation resolution and accuracy in the classification of fine spatial resolution SAR images. It is executable on a personal computer and does not require special hardware. The method is tested on four benchmark PolSAR sites and potentially extended to explore new bands. Further improvement researches investigate the combination of EM channels with image processing features within the TCN model, focusing solely on real-value EM channels. The approach achieved an accuracy of 86% in classifying the various regions, especially in dataset three, flevo_1.

### 6.1 Study Limitations

Although with quite promising results, this work has some significant limitations: the datasets used for experiments are not only on a limited scale but also lack diversity in terms of variability ranging from those experimentally found in real PolSAR data. Model performance should be further analyzed with variety more diverse datasets from different geographic locations and imaging systems. The use of preprocessed and segmented data is also helpful in that this simplifies analysis but might degrade model performance in less controlled or noisier environments. Another limitation is computational scalability of the model in terms of its ability to scale with extremely large data sizes. Though the sliding-window approach is highly conducive to a reduction in computation demands, further optimization might be needed to ensure better scalability for greater sizes of PolSAR data. This entails the use of dynamic environments, for example, real-time disaster monitoring or rapidly changing landscapes, and it leaves model performance as an untouched area of research. Finally, this approach may restrain model applicability if data distributions are highly complex and especially non-linear, for example, using a conventional classifier like SVM. The use of more complex classifiers or unsupervised techniques may open up ways towards improvement within classification outcomes. Future work should address the limitations outlined above to further validate and improve this model to even better extend its applicability across a wider range of PolSAR scenarios

## 6.2 Study Implications

From a practical viewpoint, the results of this work can be of additional interest for the remote-sensing research community and practitioners. The proposed TCN-SVM framework appeared to be a promising solution to boost the performance of PolSAR image classification in situations with restricted computational resources. This makes it viable for application in areas such as land cover mapping, environmental monitoring, and disaster management, where high classification accuracy with relatively lower computational complexity is the need. For the practitioner, streamlined processing of an approach can work to make large datasets analysis possible in reality by reducing the high demand on extensive feature extraction requirements. Therefore, good performance across various datasets also hints at an ability to adapt to different imaging conditions, which may be particularly significant for multi-regional or multi-sensor applications. Thus, the hybrid approach based on TCN, with its feature-extracting abilities combined with the robust classification ability of SVM, is promising and capable of bringing improvements in efficiency in the processing of PolSAR data. From an academic perspective, this research is added to the fast-growing literature regarding applications of machine learning in remote sensing. It gives insights into how deep learning models could be adapted to better handle high-dimensional, complex data like PolSAR imagery. It highlights how hybrid models might strike a balance between accuracy and computational efficiency, with much future innovation likely coming from this direction.

## 6.3 Future Research Trends

There are thus several paths to further research opened off from the back of this study's results. One would be to expand the analysis, using diverse datasets from different geographic regions and even imaging systems, to establish whether these findings also have applicability at more basic levels. Further performance with dynamic, real-time datasets will help to open up the applicability in operational environments like disaster response or real-time environmental monitoring. In addition to that, analyzing some of the other alternative classifiers to SVM would further enhance a sense of robustness in handling the kind of non-linear nature that the data distribution might take. Use of more advanced algorithms in machine learning could include random forests or deep learning techniques like transformers, for instance, which would classify better and be computationally efficient. Another promising avenue is the exploration of unsupervised learning, which would be a positive improvement if labeled data wasn't readily available. Finally, issues of class imbalance can be targeted in future work for those datasets that contain huge numbers of categories. Adding an attention mechanism to the architecture of TCN could introduce capabilities in more complex spatial-temporal relationships within the data, thereby boosting related classification outcomes.

## Conflicts of Interest

Declare conflicts of interest or state "The authors declare no conflicts of interest." Authors must identify and declare any personal circumstances or interest that may be perceived as inappropriately influencing the representation or interpretation of reported research results. Any role of the funders in the design of the study; in the

collection, analyses or interpretation of data; in the writing of the manuscript; or in the decision to publish the results must be declared in this section. If there is no role, please state "The funders had no role in the design of the study; in the collection, analyses, or interpretation of data; in the writing of the manuscript; or in the decision to publish the results".

## References

Ahishali, M., Kiranyaz, S., Ince, T., & Gabbouj, M. (2021). Classification of polarimetric SAR images using compact convolutional neural networks. *GIScience & Remote Sensing*, *58*(1), 28-47. https://doi.org/10.1080/15481603.2020.1853948

Al Doghan, M. A., & Piaralal, S. K. (2024). Exploring the Impact of E-Learning Initiatives on Students' Self-Efficacy and E-Learning Experiences. Eurasian Journal of Educational Research, 109(109), 158-176. https://doi.org/10.14689/ejer.2024.109.010

Cao, Y., Wu, Y., Li, M., Liang, W., & Zhang, P. (2021). PolSAR image classification using a superpixel-based composite kernel and elastic net. *Remote Sensing*, *13*(3), 380. https://doi.org/10.3390/rs13030380

Chen, J., Hou, B., Ren, B., Wu, Q., & Jiao, L. (2023). An Improved Neural Network Classification Algorithm by Expanding Training Samples for Polarimetric SAR Application. *IEEE Transactions on Geoscience and Remote Sensing*. https://doi.org/10.1109/TGRS.2023.3304115

Chicco, D., & Jurman, G. (2020). The advantages of the Matthews correlation coefficient (MCC) over F1 score and accuracy in binary classification evaluation. *BMC genomics*, *21*, 1-13. https://doi.org/10.1186/s12864-019-6413-7

Fang, Z., Zhang, G., Dai, Q., Xue, B., & Wang, P. (2023). Hybrid Attention-Based Encoder–Decoder Fully Convolutional Network for PolSAR Image Classification. *Remote Sensing*, *15*(2), 526. https://doi.org/10.3390/rs15020526

Ferreira, J. A., Rodrigues, A. K., Ospina, R., & Gomez, L. (2024). Machine learning classification based on k-Nearest Neighbors for PolSAR data. *Anais da Academia Brasileira de Ciências*, *96*(1), e20230064. https://doi.org/10.1590/0001-3765202420230064

Guo, G., & Yuan, W. (2020). Short-term traffic speed forecasting based on graph attention temporal convolutional networks. *Neurocomputing*, *410*, 387-393. https://doi.org/10.1016/j.neucom.2020.06.001

Han, W., Zhang, X., Wang, Y., Wang, L., Huang, X., Li, J., Wang, S., Chen, W., Li, X., & Feng, R. (2023). A survey of machine learning and deep learning in remote sensing of geological environment: Challenges, advances, and opportunities. *ISPRS Journal of Photogrammetry and Remote Sensing*, *202*, 87-113. https://doi.org/10.1016/j.isprsjprs.2023.05.032

Hua, W., Hou, Q., Jin, X., Liu, L., Sun, N., & Meng, Z. (2024). A Feature Fusion Network for PolSAR Image Classification Based on Physical Features and Deep Features. *IEEE Geoscience and Remote Sensing Letters*. https://doi.org/10.1109/LGRS.2024.3417929

Hua, W., Wang, C., Sun, N., & Liu, L. (2024). Multi-scale contrastive learning method for PolSAR image classification. *Journal of Applied Remote Sensing*, *18*(1), 014502-014502. https://doi.org/10.1117/1.JRS.18.014502

Imani, M. (2024). An iterative PolSAR image classification method with utilizing scattering and contextual information. *Multimedia Tools and Applications*, *83*(6), 16605-16621. https://doi.org/10.1007/s11042-023-16205-z

Karachristos, K., Koukiou, G., & Anastassopoulos, V. (2024). A Review on PolSAR Decompositions for Feature Extraction. *Journal of Imaging*, *10*(4), 75. https://doi.org/10.3390/jimaging10040075

Lara-Benítez, P., Carranza-García, M., Luna-Romera, J. M., & Riquelme, J. C. (2020). Temporal convolutional networks applied to energy-related time series forecasting. *applied sciences*, *10*(7), 2322. https://doi.org/10.3390/app10072322

Lea, C., Vidal, R., Reiter, A., & Hager, G. D. (2016). Temporal convolutional networks: A unified approach to action segmentation. Computer Vision–ECCV 2016 Workshops: Amsterdam, The Netherlands, October 8-10 and 15-16, 2016, Proceedings, Part III 14,47-54. https://doi.org/10.1007/978-3-319-49409-8_7

Li, G. (2022). From Society to Shehui: The Early Configuration of a Basic Concept in Modern China. Cultura, 19(1), 11-28. https://doi.org/10.3726/CUL012022.0002

Li, L., Zeng, J., Jiao, L., Liang, P., Liu, F., & Yang, S. (2019). Online active extreme learning machine with discrepancy sampling for PolSAR classification. *IEEE Transactions on Geoscience and Remote Sensing*, *58*(3), 2027-2041. https://doi.org/10.1109/TGRS.2019.2952236

McHugh, M. L. (2012). Interrater reliability: the kappa statistic. *Biochemia medica*, *22*(3), 276-282. https://hrcak.srce.hr/89395

Meng, L., Yan, C., Lv, S., Sun, H., Xue, S., Li, Q., Zhou, L., Edwing, D., Edwing, K., & Geng, X. (2024). Synthetic aperture radar for geosciences. *Reviews of Geophysics*, *62*(3), e2023RG000821. https://doi.org/10.1029/2023RG000821

Moon, W. M., Staples, G., Kim, D.-j., Park, S.-E., & Park, K.-A. (2010). RADARSAT-2 and coastal applications: Surface wind, waterline, and intertidal flat roughness. *Proceedings of the IEEE*, *98*(5), 800-815. https://doi.org/10.1109/JPROC.2010.2043331

Pollachom, T., Kongyok, C., Mueangkaew, K., Thasrabiab, T., & Boripis, T. (2022). Hijab: The influence of THE Islamic revivalist movement on muslim women in southernmost provinces of thailand. Przestrzeń Społeczna (Social Space). http://hdl.handle.net/123456789/4147

Qiao, H., Zhang, P., Li, Z., Huang, L., Gao, S., Liu, C., Wu, Z., Liang, S., Zhou, J., & Sun, W. (2024). A new snow depth retrieval method by improved hybrid DEM differencing and coherence amplitude algorithm for PolInSAR. *Journal of Hydrology*, *628*, 130507. https://doi.org/10.1016/j.jhydrol.2023.130507

Shabayek, D. A., Rimbawan, R., & Budijanto, S. (2022). The potential of red kidney beans and brown rice-based flakes for breakfast to reduce obesity. Future Of Food. https://dx.doi.org/doi:10.17170/kobra-202110144903

Shokr, M., & Dabboor, M. (2023). Polarimetric SAR applications of sea ice: A review. *IEEE Journal of Selected Topics in Applied Earth Observations and Remote Sensing*. https://doi.org/10.1109/JSTARS.2023.3295735

Übeyli, E. D. (2007). ECG beats classification using multiclass support vector machines with error correcting output codes. *Digital Signal Processing*, *17*(3), 675-684. https://doi.org/10.1016/j.dsp.2006.11.009

Wang, Z., Zeng, X., Yan, Z., Kang, J., & Sun, X. (2022). AIR-PolSAR-Seg: A large-scale data

set for terrain segmentation in complex-scene PolSAR images. *IEEE Journal of Selected Topics in Applied Earth Observations and Remote Sensing*, *15*, 3830-3841. https://doi.org/10.1109/JSTARS.2022.3170326

Yadav, K., Arora, A., Yadav, R., & Saini, C. P. (2022). Gamified Apps and Customer Engagement: Modeling in Online Shopping Environment. Transnational Marketing Journal, 10(3), 593-605. https://doi.org/10.33182/tmj.v10i3.2199

Yang, C., Hou, B., Ren, B., Liu, X., Chanussot, J., Wang, S., & Jiao, L. (2024). SSDFL: Spatial scattering decomposition feature learning for PolSAR image. *International Journal of Applied Earth Observation and Geoinformation*, *128*, 103702. https://doi.org/10.1016/j.jag.2024.103702

Zhang, T., Long, J., Lin, H., Liu, Z., Ye, Z., & Zheng, H. (2024). A Novel Feature Evaluation Method in Mapping Forest AGB by Fusing Multiple Evaluation Metrics Using PolSAR Data. *IEEE Geoscience and Remote Sensing Letters*, *21*, 1-5. https://doi.org/10.1109/LGRS.2024.3378425

Zou, C., Dong, D., Wang, S., Li, J., Li, X., Wang, Y., Li, D., & Cheng, K. (2010). Geological characteristics and resource potential of shale gas in China. *Petroleum exploration and development*, *37*(6), 641-653. https://doi.org/10.1016/S1876-3804(11)60001-3